Molecular Orbital Gates for Plasmon Excitation

Theresa Lutz,[†,#] Christoph Große,*[,†,#] Christian Dette,[†] Alexander Kabakchiev,[†] Frank Schramm,[‡] Mario Ruben,[‡,§] Rico Gutzler,[†] Klaus Kuhnke,[†] Uta Schlickum,*[,†] and Klaus Kern[†,‖]

[†]Max-Planck-Institut für Festkörperforschung, Heisenbergstraße 1, 70569 Stuttgart, Germany
[‡]Karlsruher Institut für Technologie (KIT), Institut für Nanotechnologie, 76344 Eggenstein-Leopoldshafen, Germany
[§]IPCMS-CNRS, Université de Strasbourg, 67034 Strasbourg, France
[‖]Institut de Physique de la Matière Condensée, Ecole Polytechnique Fédérale de Lausanne, 1015 Lausanne, Switzerland

Ⓢ Supporting Information

ABSTRACT: Future combinations of plasmonics with nanometer-sized electronic circuits require strategies to control the electrical excitation of plasmons at the length scale of individual molecules. A unique tool to study the electrical plasmon excitation with ultimate resolution is scanning tunneling microscopy (STM). Inelastic tunnel processes generate plasmons in the tunnel gap that partially radiate into the far field where they are detectable as photons. Here we employ STM to study individual tris-(phenylpyridine)-iridium complexes on a C_{60} monolayer, and investigate the influence of their electronic structure on the plasmon excitation between the Ag(111) substrate and an Ag-covered Au tip. We demonstrate that the highest occupied molecular orbital serves as a spatially and energetically confined nanogate for plasmon excitation. This opens the way for using molecular tunnel junctions as electrically controlled plasmon sources.

KEYWORDS: Molecular orbitals, STM, STM-induced luminescence, plasmons, Ir(ppy)₃, organic molecules
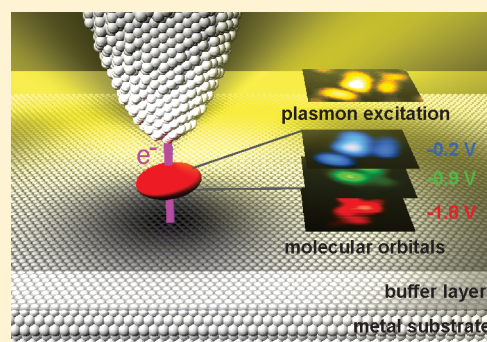
Exploiting the collective electron oscillations (surface plasmon polaritons) at the interfaces of metallic nanostructures has enabled guiding and manipulating light on subwavelength scales[1,2] and allowed various technologically relevant applications like signal-processing plasmonic circuits[3] or plasmonic sensors.[4] While the excitation in these devices is typically induced by incident light, their integration into conventional electronic circuits would require direct interfaces between nanoelectronics and nanophotonics, as well as strategies to generate plasmons electrically. However, the direct excitation of plasmons by high energy electron beams[5,6] is difficult to implement in compact devices. A feasible alternative approach is the excitation of gap plasmons at tunnel junctions addressing the plasmonic structures.[7,8] The mechanisms determining the excitation of localized plasmons at plain metal surfaces and metallic nanostructures have been extensively investigated by scanning tunneling microscopy (STM).[9–12] This experimental technique employs the close proximity (∼1 nm) between the analyzed surface and a metallic tip, together with the highly localized tunnel current, to probe the local excitation of plasmons with atomic precision.[12] The created gap plasmons are excited by the tunnel current[9,10] and either couple to propagating surface plasmons or radiate as photons.[7,8] Detecting the intensity of these photons in the far field as a function of tip position leads to so-called photon maps[10,12–16] that display the local excitation efficiency of plasmons.

Introducing individual molecules into the tunnel junction modifies the plasmonic emission with respect to spectral shape and intensity. Three major mechanisms have been discussed to describe the influence of the molecules. (I) They modify the efficiency of the inelastic tunnel process leading to plasmon excitation by changing the density of initial or final states[14,15,17] or the matrix element;[14] (II) molecules left in an excited state enhance plasmon modes due to their dynamic dipole,[18–22] and (III) the dielectric properties of the molecules and the junction geometry alter the field strength of the tip-induced plasmon modes.[14,16,18–24] Besides the radiation of plasmons, additional photons can be generated by intramolecular transitions, that is, the recombination of electrons and holes injected into the molecules, when the molecules are electronically decoupled from the metal substrate by a few atomic layers of an insulator[25,26] or molecular multilayers.[27,28] An excellent introduction to STM-induced luminescence appeared in 2010.[29]

The critical assessment of the different mechanisms and their control is decisive for the application of single molecules as ultimate coupling elements for the electrical plasmon generation. Apart from recording optical and differential conductance (dI/dV) spectra, we use the ability of STM to

image individual molecular orbitals[30−32] and analyze the local excitation of plasmons in terms of the present molecular states. The additional spatial information unequivocally proves that molecular orbitals can be exploited to confine plasmon excitation spatially and energetically.

Our model system consists of single *fac*-tris(2-phenyl-pyridine)iridium(III) admolecules (Ir(ppy)$_3$) deposited on a C$_{60}$ monolayer acting as a molecular buffer layer to the Ag(111) substrate (Figure 1a). The buffer layer reduces the electronic
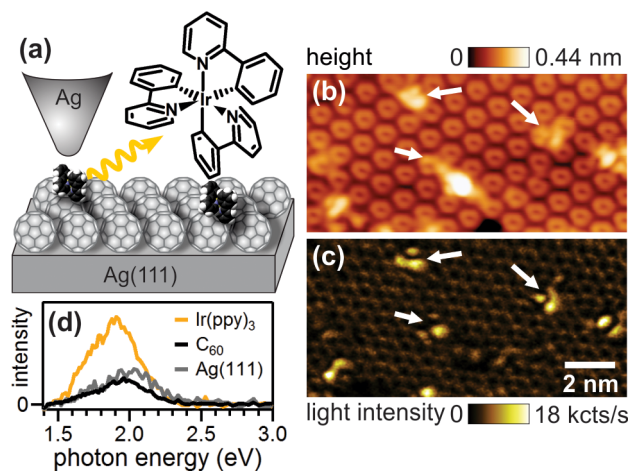

Figure 1. Overview of the investigated system. (a) Experimental setup and sketch of the Ir(ppy)$_3$ admolecules on top of a C$_{60}$ monolayer grown on Ag(111). (b) Constant current STM topograph of Ir(ppy)$_3$ admolecules on C$_{60}$, and (c) simultaneously recorded photon map. The arrows indicate individual Ir(ppy)$_3$ molecules. (d) Luminescence spectrum taken on a single Ir(ppy)$_3$ molecule (yellow), on the C$_{60}$ monolayer (black), and on the pristine Ag(111) substrate (gray). Both the images in b and c and the optical spectra in d were recorded at a tunnel current of 20 pA and a bias voltage of −3.0 V.

coupling between the molecular states and the metal substrate.[30] In contrast, a direct adsorption of the single Ir(ppy)$_3$ molecules on Ag(111) leads to a strong distortion of the molecular states (see Supporting Information, Figure S1).

In STM topographs (Figure 1b) individual Ir(ppy)$_3$ admolecules appear as protrusions on the perfectly ordered C$_{60}$ layer. The simultaneously recorded photon map (Figure 1c) represents the spectrally integrated luminescence intensity detected by a single photon counting detector. While there is only weak light emission on the C$_{60}$ layer, on Ir(ppy)$_3$ molecules a well-defined, submolecular structured light pattern with fourfold increased intensity is observed. The occurrence of three differently shaped submolecular patterns (arrows in Figure 1c) are ascribed to different adsorption geometries on the underlying C$_{60}$ lattice. Figure 1d displays typical optical spectra on top of a single Ir(ppy)$_3$ molecule, on the C$_{60}$ monolayer and on the pristine Ag(111) substrate. The specific shape and width of the spectra strongly depends on the geometry of the tip (see Supporting Information, Figure S3). The fact that spectra on the Ir(ppy)$_3$ molecules show similarly broad features as the ones on Ag(111) without a molecule-specific fine structure strongly suggests a plasmonic origin of the emitted light. This point will, however, be discussed in more detail below.

The submolecular pattern in the photon map (Figure 1c) and the topographic appearance (Figure 1b) of the molecules are markedly different. This becomes particularly apparent in

Figure 2a,b which depicts a single Ir(ppy)$_3$ molecule. To explore the relation between the light excitation pattern and the
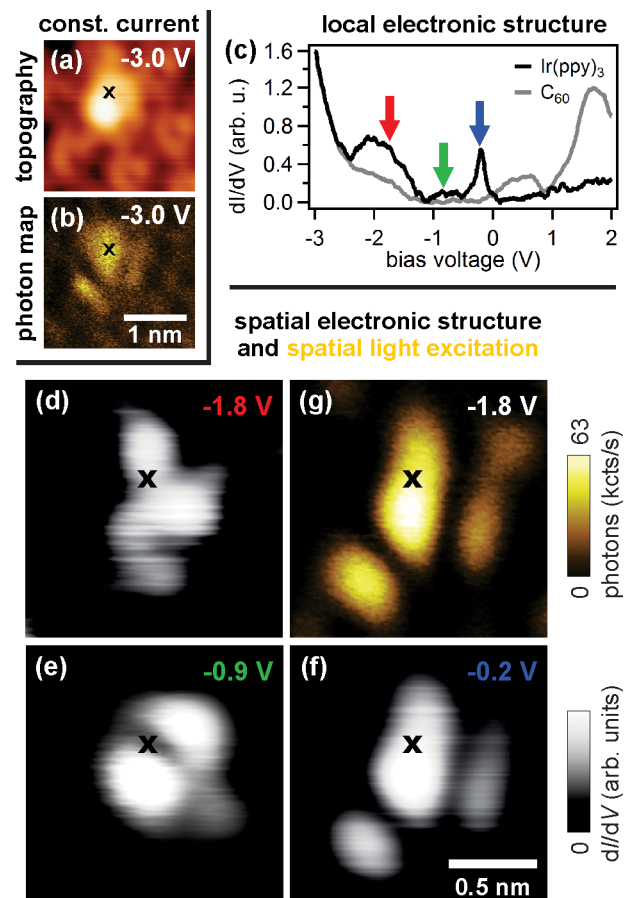

Figure 2. Electronic and luminescence characteristics of a single Ir(ppy)$_3$ molecule. (a) Constant current STM topograph and (b) simultaneously recorded photon map (tunnel current: 20 pA). (c) Differential conductance (dI/dV) spectra taken on Ir(ppy)$_3$ (black, spatial position marked by X in the other images) and on the C$_{60}$ layer (gray). (d−f) dI/dV maps recorded in constant height mode at the three indicated bias voltages. (g) Photon map recorded simultaneously with d.

electronic structure, that is, the molecular orbitals, we probe the local density of states (Figure 2c−f) as a function of energy (bias voltage) by dI/dV spectra (Figure 2c, black curve) and spatially by dI/dV maps (Figure 2d−f). dI/dV spectra on Ir(ppy)$_3$ molecules exhibit three distinct peaks at −1.8, −0.9, and −0.2 V (for details see Supporting Information, Figure S2). Minor variations of a few tenths of an eV are found for different molecules due to varying adsorption geometries. We assign the state closest to the Fermi energy at −0.2 V to the highest occupied molecular orbital (HOMO) of the adsorbed species. In the positive voltage range, neither Ir(ppy)$_3$-specific electronic states nor an enhanced plasmon excitation is observed up to +3.0 V (see Supporting Information, Figure S3). dI/dV spectra on the C$_{60}$ buffer layer (Figure 2c, gray curve) perfectly agree with the literature[33] and show that the −0.2 and −0.9 V Ir(ppy)$_3$ states lie in the C$_{60}$ band gap. For bias voltages beyond −1.6 V a spatially defined light pattern with substantial intensity appears which does not change its general shape up to −3.0 V (Figure 2b,g). A comparison of the photon map at −1.8 V with the simultaneously recorded
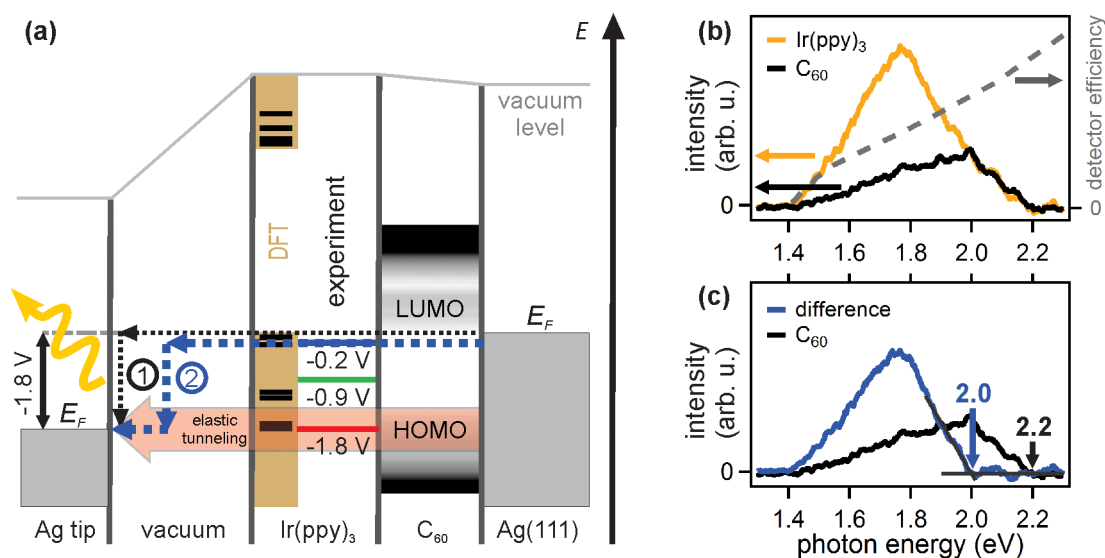
Figure 3. Energy level diagram and luminescence spectra. (a) Energy levels of the investigated system for a bias voltage of −1.8 V. The experimentally observed Ir(ppy)$_3$ states are displayed as color-coded lines (compare to arrows in Figure 2c), the calculated values (see Supporting Information, Figure S4) as black lines in the ocher-colored box. ① and ② represent two inelastic tunnel paths resulting in plasmonic light emission on single Ir(ppy)$_3$ molecules. (b) Photon spectra recorded at a bias voltage of −2.2 V on Ir(ppy)$_3$ (yellow) and on C$_{60}$ (black). The dashed gray line depicts the quantum efficiency of the intensified detector. (c) Difference (blue) between the spectra in b contrasted with the spectrum on C$_{60}$ (black). The respective high-energy cutoff of the two spectra is marked by arrows.

molecular orbital (Figure 2d) confirms their marked difference. However, the light pattern shows a clear similarity to the shape of the HOMO at −0.2 V (Figure 2f). For the varying adsorption geometries mentioned above, we always find a clear congruence between the pattern of the enhanced light intensity and the shape of the orbital closest to the Fermi level.

To explain this observation, we consider the energy level scheme of the studied system (Figure 3a) derived from the identified molecular levels. For comparison, the figure additionally contains the energy levels obtained from density functional theory (DFT) calculations of free Ir(ppy)$_3$ molecules, assuming a vacuum level alignment with the C$_{60}$-covered Ag(111) surface (work function: 5 eV,[34,35] for details see Supporting Information, Figure S4). The energetic positions of these levels agree well with the experimental data. At a bias voltage of −1.8 V, the main tunnel current passes through the C$_{60}$ HOMO. However, the excitation of plasmons (i.e., the recorded luminescence) stems from two main inelastic tunnel processes. Path ① occurs due to electrons which tunnel inelastically from the substrate to the tip without involving Ir(ppy)$_3$ states. On the Ir(ppy)$_3$ molecules, the presence of the HOMO opens an energetically and spatially defined gate that significantly enhances the tunnel process at this energy (path ②). As a consequence, more tunneling electrons are available with a sufficient energy to excite plasmons in the visible range, which results in the locally enhanced luminescence. Since the spatial shape of the HOMO defines this gate, the photon map always matches the dI/dV map at −0.2 V. The lower-lying Ir(ppy)$_3$ orbitals play no significant role in the luminescence excitation process. This observation is a clear evidence for the plasmonic origin of the generated photons. A radiative intramolecular transition, in contrast, would require the simultaneous injection of an electron and a hole into the molecule. At negative bias voltages as used here, the hole is injected by the tip, whereas the electron injection occurs from the substrate. Since only the hole injection depends on the spatial position of the tip, the photon map

should display the orbital into which the hole is injected. For a radiative intramolecular transition this would be the −1.8 V orbital, which is clearly not observed in the photon map. With a similar argument we can also exclude a possible resonance of excited plasmon modes with pre-existing electron−hole pairs because this would result in a superposition of the −0.2 and −1.8 V orbital in the photon map. Moreover, such a second-order process requiring one electron to create the electron−hole pair and a second one to induce the plasmon is not compatible with the perfectly linear dependence of the luminescence intensity with the tunnel current (see Supporting Information, Figure S5).

Consequently, the comparison of submolecular resolved photon maps with the spatial shape of the molecule's orbitals provides strong evidence for the involved luminescence process. This is important since it may corroborate arguments obtained from optical spectra of the emitted light, such as their width[15−23] or the observation of vibrational progressions.[22,25−27]

In order to independently verify the two-path scheme discussed above, we recorded luminescence spectra at electron energies that are small enough to impose a sharp intensity cutoff within the broad plasmon spectrum. Figure 3b presents two optical spectra recorded at −2.2 V bias, one on an Ir(ppy)$_3$ admolecule (yellow) and the other one on the C$_{60}$ layer (black). By alternatingly recording several spectra on the single molecule and the C$_{60}$ layer, we can exclude any change of the tip. Both spectra exhibit a high-energy quantum cutoff at 2.2 eV which results from the maximum possible electron energy loss at the tunnel voltage of −2.2 V. The continuous intensity reduction at low energies arises from the diminishing quantum efficiency of the intensified detector (dashed gray line, Figure 3b). When normalizing the spectra in the quantum cutoff region, it becomes obvious that the spectra recorded on Ir(ppy)$_3$ show a significantly stronger contribution at smaller photon energies. Figure 3c displays the difference (blue curve) between the spectrum on the Ir(ppy)$_3$ molecule and on the C$_{60}$

layer. The 0.2 eV lower cutoff energy of this difference spectrum compared to the C_{60} spectrum (Figure 3c, black curve) is in perfect agreement with the energetic position of the HOMO and thus corroborates the mechanism discussed above.

Our results clearly demonstrate that resolving both the discrete energy levels of molecules and the local light excitation with submolecular spatial resolution allows identifying the inelastic tunnel channels responsible for plasmonic excitation. The enhanced intensity and the significant spectral shift on the admolecules can be explained by their electronic structure. For the studied system, intramolecular transitions and dielectric properties may be of minor importance. With an analogue mechanism it is also possible to elucidate the luminescence process on the C_{60} monolayer directly adsorbed on the metal surface (see Supporting Information, Figure S7).

This study reveals that single molecules located in a tunnel junction act as energetically and submolecularly defined spatial gates for the electrical excitation of plasmons and the emitted luminescence. The intensity and spectral distribution of the generated plasmons are directly related to the spatial shape and the energy of the orbital closest to the Fermi energy. Transferring this concept to other adsorbate systems with known orbital properties may offer the possibility to directly control the electrical excitation of plasmons in a predictable manner. This paves the way for new plasmon and light sources, for example for the direct integration of plasmonics into electronic circuits. Furthermore, the observed relationship between the excited plasmons and the molecular orbitals may provide an efficient way to follow fundamental molecular processes, like charging processes or conformational changes, by exploiting the radiation of plasmons as an ultrafast read-out signal.

Methods. The experiments were performed in a low temperature (≈ 5 K) scanning tunneling microscope working in an ultrahigh vacuum environment ($<10^{-10}$ mbar) that is equipped with three independent optical access paths to the tunnel junction, as described elsewhere.[36] Using two of these paths, optical spectroscopy and spectrally integrated photon counting can be employed simultaneously. dI/dV spectra and dI/dV maps are recorded by modulating the bias voltage (20 mV, 524 Hz) and using lock-in detection. In Figure 2 the lateral drift between the different images and the depicted position of the dI/dV spectrum was corrected by linearly fitting the position of the lower left HOMO lobe of eight different images (x-drift: −51 pm/h, y-drift: −118 pm/h). Bias voltages refer to the sample voltage with respect to the tip.

To enhance the plasmon-mediated luminescence, the STM tips are prepared by evaporating silver onto electrochemically etched Au tips.[11] For the preparation of the samples approximately 1 ML of C_{60} is deposited from an effusion cell on a clean and atomically flat Ag(111) crystal surface. The C_{60} layer forms a well-ordered, hexagonal close-packed molecular structure.[33] Subsequently, a submonolayer coverage of Ir(ppy)$_3$ molecules is deposited on top of the C_{60} monolayer. The entire deposition is carried out with the substrate held at room temperature. Ir(ppy)$_3$ is synthesized according to a literature report.[37,38] The respective analytical and spectral data correspond to the reported values. Final purification after column chromatography of the reaction material (SiO_2, CH_2Cl_2) was achieved by vacuum sublimation (180 °C, 2 × 10^{-3} mbar). The nondestructive evaporation of Ir(ppy)$_3$ molecules was proved by laser desorption−ionization mass spectra of evaporated Ir(ppy)$_3$ films.

ASSOCIATED CONTENT

S Supporting Information

STM image and dI/dV spectra of single Ir(ppy)$_3$ molecules directly adsorbed on Ag(111), dI/dV spectra of single Ir(ppy)$_3$ molecules on C_{60} monolayer/Ag(111), density functional theory calculation of Ir(ppy)$_3$, optical spectra on the C_{60} monolayer and single Ir(ppy)$_3$ molecules on top obtained with different tips, luminescence intensity on single Ir(ppy)$_3$ molecules as a function of tunnel current, and plasmon excitation on the C_{60} monolayer. This material is available free of charge via the Internet at http://pubs.acs.org.

AUTHOR INFORMATION

Corresponding Author
*E-mail: c.grosse@fkf.mpg.de; u.schlickum@fkf.mpg.de.

Author Contributions
#T.L. and C.G. contributed equally to this work.

Notes
The authors declare no competing financial interest.

ACKNOWLEDGMENTS

ABBREVIATIONS

DFT, density functional theory; dI/dV maps, differential conductance maps; dI/dV spectra, differential conductance spectra; Ir(ppy)$_3$, fac-tris(2-phenylpyridine)iridium(III); HOMO, highest occupied molecular orbital; LUMO, lowest unoccupied molecular orbital; STM, scanning tunneling microscopy

REFERENCES

(1) Schuller, J. A.; Barnard, E. S.; Cai, W.; Jun, Y. C.; White, J. S.; Brongersam, M. L. *Nat. Mater.* **2010**, *9* (3), 193−204.
(2) Gramotnev, D. K.; Bozhevolnyi, S. *Nat. Photonics* **2010**, *4* (2), 83−91.
(3) Ozbay, E. *Science* **2006**, *311* (5758), 189−193.
(4) Anker, J. N.; Hall, W. P.; Lyandres, O.; Shah, N. C.; Zhao, J.; Van Duyne, R. P. *Nat. Mater.* **2008**, *7* (6), 442−453.
(5) Bashevoy, M.; Jonsson, F.; Krasavin, A.; Zheludev, N.; Chen, Y.; Stockman, M. *Nano Lett.* **2006**, *6* (6), 1113−1115.
(6) Rossouw, D.; Couillard, M.; Vickery, J.; Kumacheva, E.; Botton, G. A. *Nano Lett.* **2011**, *11* (4), 1499−1504.
(7) Bharadwaj, P.; Bouhelier, A.; Novotny, L. *Phys. Rev. Lett.* **2011**, *106* (22), 226802.
(8) Wang, T.; Boer-Duchemin, E.; Zhang, Y.; Comtet, G.; Dujardin, G. *Nanotechnology* **2011**, *22*, 175201.
(9) Gimzewski, J. K.; Sass, J. K.; Schlitter, R. R.; Schott, J. *Europhys. Lett.* **1989**, *8* (5), 435−440.
(10) Berndt, R.; Gimzewski, J. K.; Johansson, P. *Phys. Rev. Lett.* **1991**, *67* (27), 3796−3799.
(11) Berndt, R.; Gimzewski, J. K. *Phys. Rev. Lett.* **1993**, *71* (21), 3493−3496.
(12) Berndt, R.; Gaisch, R.; Schneider, W.-D.; Gimzewski, J. K.; Reihl, B.; Schlittler, R. R.; Tschudy, M. *Phys. Rev. Lett.* **1995**, *74* (1), 102−105.
(13) Sakurai, M.; Thirstrup, C.; Aono, M. *Appl. Phys. A: Mater. Sci. Process.* **2005**, *80* (6), 113−1160.
(14) Berndt, R.; Gimzewski, J. K. *Phys. Rev. B* **1993**, *48* (7), 4746−4754.

(15) Geng, F.; Zhang, Y.; Yu, Y.; Kuang, Y.; Liao, Y.; Dong, Z.; Hou, J. *Opt. Express* **2012**, *20* (24), 26725−26735.

(16) Hoffmann, G.; Libioulle, L.; Berndt, R. *Phys. Rev. B* **2002**, *65* (21), 212107.

(17) Schneider, N. L.; Matino, F.; Schull, G.; Gabutti, S.; Mayor, M.; Berndt, R. *Phys. Rev. B* **2011**, *84* (15), 153403.

(18) Guo, X. L.; Dong, Z. C.; Trifonov, A. S.; Mashiko, S.; Okamoto, T. *Phys. Rev. B* **2003**, *68* (11), 113403.

(19) Zhang, Y.; Tao, X.; Gao, H. Y.; Dong, Z. C.; Hou, J. G.; Okamoto, T. *Phys. Rev. B* **2009**, *79* (7), 075406.

(20) Zhang, Y.; Geng, F.; Gao, H. Y.; Liao, Y.; Dong, Z. C.; Hou, J. G. *Appl. Phys. Lett.* **2010**, *97* (24), 243101.

(21) Dong, Z. C.; Kar, A.; Dorozhkin, P.; Amemiya, K.; Uchihashi, T.; Yokoyama, S.; Kamikado, T.; Mashiko, S.; Okamoto, T. *Thin Solid Films* **2003**, *438* (0), 262−267.

(22) Dong, Z. C.; Trifonov, A. S.; Guo, X. L.; Amemiya, K.; Yokoyama, S.; Kamikado, T.; Yamada, T.; Mashiko, S.; Okamoto, T. *Surf. Sci.* **2003**, *532*, 237−243.

(23) Rossel, F.; Pivetta, M.; Patthey, F.; Schneider, W.-D. *Opt. Express* **2009**, *17* (4), 2714−2721.

(24) Tao, X.; Dong, Z. C.; Yang, J. L.; Luo, Y.; Hou, J. G.; Aizpurua, J. *J. Chem. Phys.* **2009**, *130* (8), 084706.

(25) Qiu, X. H.; Nazin, G. V.; Ho, W. *Science* **2003**, *299* (5606), 542−546.

(26) Ćavar, E.; Blüm, M.-C.; Pivetta, M.; Patthey, F.; Chergui, M.; Schneider, W.-D. *Phys. Rev. Lett.* **2005**, *95* (19), 196102.

(27) Dong, Z. C.; Guo, X. L.; Trifonov, A. S.; Dorozhkin, P. S.; Miki, K.; Kimura, K.; Yokoyama, S.; Mashiko, S. *Phys. Rev. Lett.* **2004**, *92* (8), 086801.

(28) Kabakchiev, A.; Kuhnke, K.; Lutz, T.; Kern, K. *Chem. Phys. Chem.* **2010**, *11* (16), 3412−3416.

(29) Rossel, F.; Pivetta, M.; Schneider, W.-D. *Surf. Sci. Rep.* **2010**, *65* (5), 129.

(30) Repp, J.; Meyer, G.; Stojkovic, S. M.; Gourdon, A.; Joachim, C. *Phys. Rev. Lett.* **2005**, *94* (2), 026803.

(31) Lu, X.; Grobis, M.; Khoo, K. H.; Louie, S. G.; Crommie, M. F. *Phys. Rev. Lett.* **2003**, *90* (9), 096802.

(32) Pascual, J. I.; Gomez-Herrero, J.; Rogero, C.; Baro, A. M.; Sanchez-Portal, D.; Artacho, E.; Ordejon, P.; Soler, J. M. *Chem. Phys. Lett.* **2000**, *321* (1−2), 78−82.

(33) Altman, E. I.; Colton, R. J. *Phys. Rev. B* **1993**, *48* (24), 18244−18249.

(34) Zerweck, U.; Loppacher, C.; Otto, T.; Grafström, S.; Eng, L. M. *Nanotechnology* **2007**, *18* (8), 084006.

(35) Wang, L.-L.; Cheng, H.-P. *Phys. Rev. B* **2004**, *69* (16), 165417.

(36) Kuhnke, K.; Kabakchiev, A.; Stiepany, W.; Zinser, F.; Vogelgesang, R.; Kern, K. *Rev. Sci. Instrum.* **2010**, *81* (11), 113102.

(37) McGee, K. A.; Mann, K. R. *Inorg. Chem.* **2007**, *46* (19), 7800−7809.

(38) Nonoyama, M. *Bull. Chem. Soc. Jpn.* **1974**, *47* (3), 767−768.